

Asking photons where have they been

A. Danan, D. Farfurnik, S. Bar-Ad, and L. Vaidman
*Raymond and Beverly Sackler School of Physics and Astronomy
 Tel-Aviv University, Tel-Aviv 69978, Israel*

We present surprising experimental evidence regarding the past of photons passing through an interferometer. The information about the positions through which the photons pass in the interferometer is retrieved from modulations of the detected signal at the vibration frequencies of mirrors the photons bounce off. From the analysis we conclude that the past of the photons is not represented by continuous trajectories, although a “common sense” analysis adopted in various *welcher weg* measurements, delayed-choice which-path experiments and counterfactual communication demonstrations yields a single trajectory. The experimental results have a simple explanation in the framework of the two-state vector formalism of quantum theory.

Quantum mechanics does not provide a clear answer to the question: What was the past of a photon which went through an interferometer [1]? Various *welcher weg* measurements [2], delayed-choice which-path experiments [3–5] and weak-measurements of photons in interferometers [6–8] presented the past of a photon as a trajectory or a set of trajectories. We have carried out experimental weak measurements of the paths of photons going through a nested Mach-Zehnder interferometer, discussed earlier in another context [9, 10], which show a different picture: the past of a photon is not a set of continuous trajectories. The photons tell us that they have been in the parts of the interferometer through which they could not pass! Our results lead to rejection of a “common sense” approach to the past of a quantum particle. On the other hand they have a simple explanation within the framework of the two-state vector formalism of quantum theory [11, 12].

The experiment is analogous to the following scenario: If our radio plays Bach, we know that the photons come from a classical music station, but if we hear a traffic report, we know that the photons come from a local radio station. We can deduce where the photons were on the basis of the information they provide.

In our experiment we vibrate various mirrors inside the interferometer at different frequencies. The rotation of a mirror causes a vertical shift of the light beam reflected off that mirror. We measure the position of photons coming out of the interferometer, and Fourier-analyze the output signal. When the vibration frequency of a certain mirror appears in the power spectrum, we conclude that photons have been near that particular mirror. The vertical displacement of the beam due to the rotation of the mirrors is significantly smaller than the width of the beam, and the change in the optical path length is much smaller than the wavelength. This ensures that the disruption of the interference in the experiment is negligible.

We start with a Mach-Zehnder interferometer (MZI) aligned in such a way that every photon ends up in detector D , see Fig. 1A. Mirrors A and B vibrate around their horizontal axes at frequencies f_A and f_B respectively, causing an oscillation of the vertical position of the photons reaching the detector. The detector D is a quad-cell photo-detector, and the measured signal is the difference of the currents generated in its upper and lower cells. As expected, the power spectrum shows two equal contributions at frequencies f_A and f_B .

This observation does not answer the question: Did each photon pass through a single arm or through both arms of the interferometer? While the quantum wave of the photon passed through both arms, our measurement does not prove it. The observed current was created by numerous photons, so conceivably different ones were responsible for the two peaks of the power spectrum. Nevertheless, the measurements provide a conclusive evidence that at least some of the observed photons passed near mirrors A and B .

We also measure the signal from the detector when the second beam splitter is removed, transforming the experiment to a which-path measurement, Fig. 1B. Only the signal with frequency f_B remains.

Next, we build a larger interferometer, Fig. 2A, in which one third of the beam power goes to the lower arm and two thirds of the beam power pass through the interferometer we just described, in the upper arm. We align the inner (nested) interferometer and the large interferometer in such a way, that again all the photons end up in detector D . We vibrate all the mirrors around their horizontal axes with equal (small) amplitudes, each at a different frequency. As expected, the power spectrum shows peaks at all frequencies, and the peaks at frequencies f_E and f_F are higher than the rest.

The surprising result is obtained when the interferometer is modified to be a which-path experiment, using the nested MZI as a switch. By slightly shifting mirror B we align the MZI so that there is complete destructive interference of the light propagating towards mirror F , see Fig. 2B. In that case observing photons at D supposedly implies that those photons chose the lower arm of the interferometer. We thus expect that the photons reaching detector D have interacted only with mirror C , and that the measured signal should therefore show only the frequency f_C . Yet the

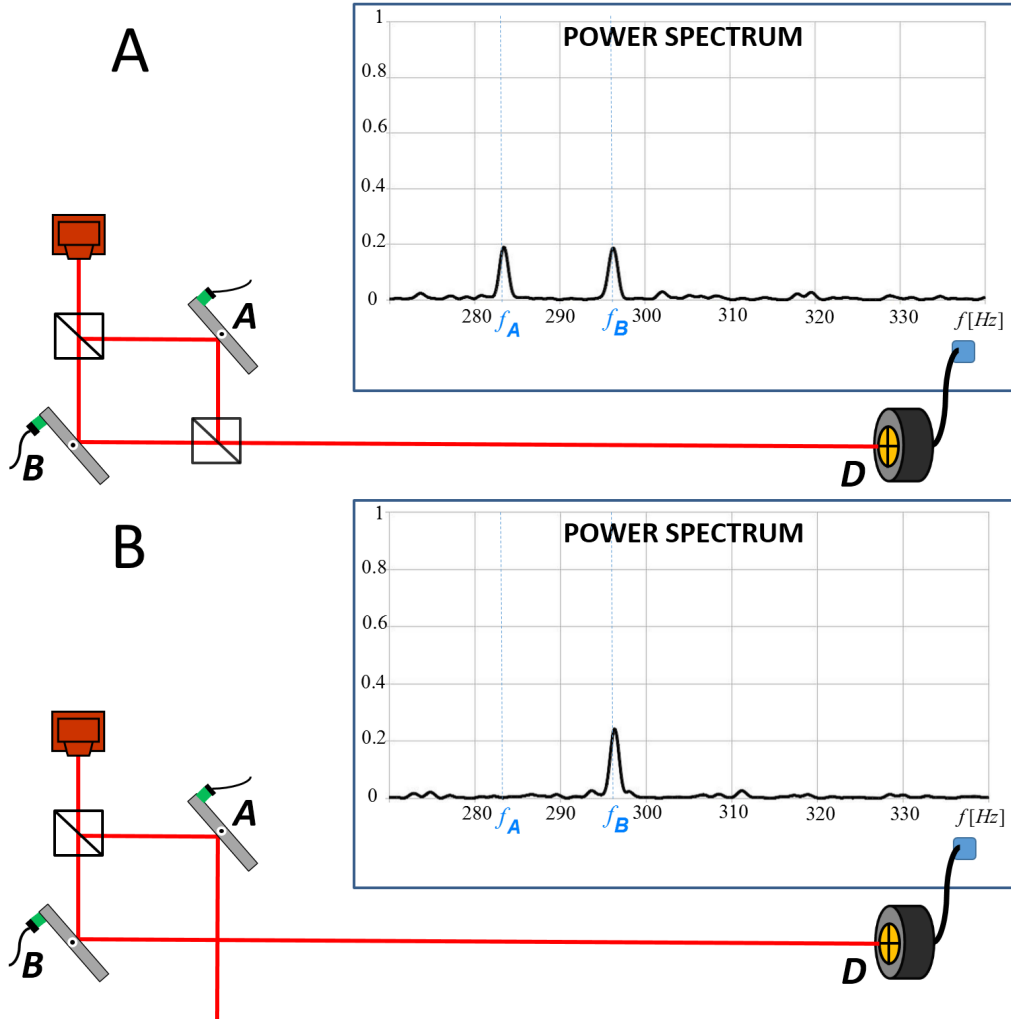


FIG. 1: (A) Measured power spectrum of the signal from the quad-cell photo-detector shows frequencies of oscillation of internal mirrors A and B of the Mach-Zehnder interferometer. (B) Only the frequency of the mirror B remains in the power spectrum of the signal when the second beam splitter of the interferometer is taken out.

results of the experiment are different: we observe *three* peaks of approximately the same strength: the expected one at frequency f_C , and two more peaks at frequencies f_A and f_B . The photons tell us that they also interacted with the mirrors of the nested interferometer in the upper arm! To verify the destructive interference of the light directed towards mirror F we blocked the lower arm, see Fig. 2C. The result was a null signal with no peaks at all. Another surprising feature of the power spectrum of Fig. 2B is the presence of peaks at f_A and f_B and the absence of peaks at f_E and f_F . The photons passing through the inner interferometer have to be reflected off the mirrors E and F and thus they are expected to yield even higher peaks at frequencies f_E and f_F .

The intuitive picture which allows to foresee and explain these results is given by the two-state vector formulation (TSVF) of quantum mechanics [11, 12]. The observed behavior applies equally if the experiment is performed with single photons [13] or with a macroscopic number of photons. In the TSVF each photon observed by detector D is described by the backward-evolving quantum state $\langle \Phi |$ created at the detector, in addition to the standard, forward-evolving wave function $|\Psi\rangle$ created at the source. The equations of the TSVF imply that a photon can have a local observable effect only if both the forward- and backward-evolving quantum waves are non-vanishing at this location. Fig. 3. shows the forward and the backward evolving states inside the interferometer in the setup of Fig. 2B. It does explain the peculiar features of the power spectrum. The peaks at frequencies f_A , f_B , and f_C correspond to the fact that near mirrors A , B , and C both forward evolving and backward evolving quantum states are present. The absence of the peak at f_E follows from the absence of the backward evolving wave near E while the absence of the forward

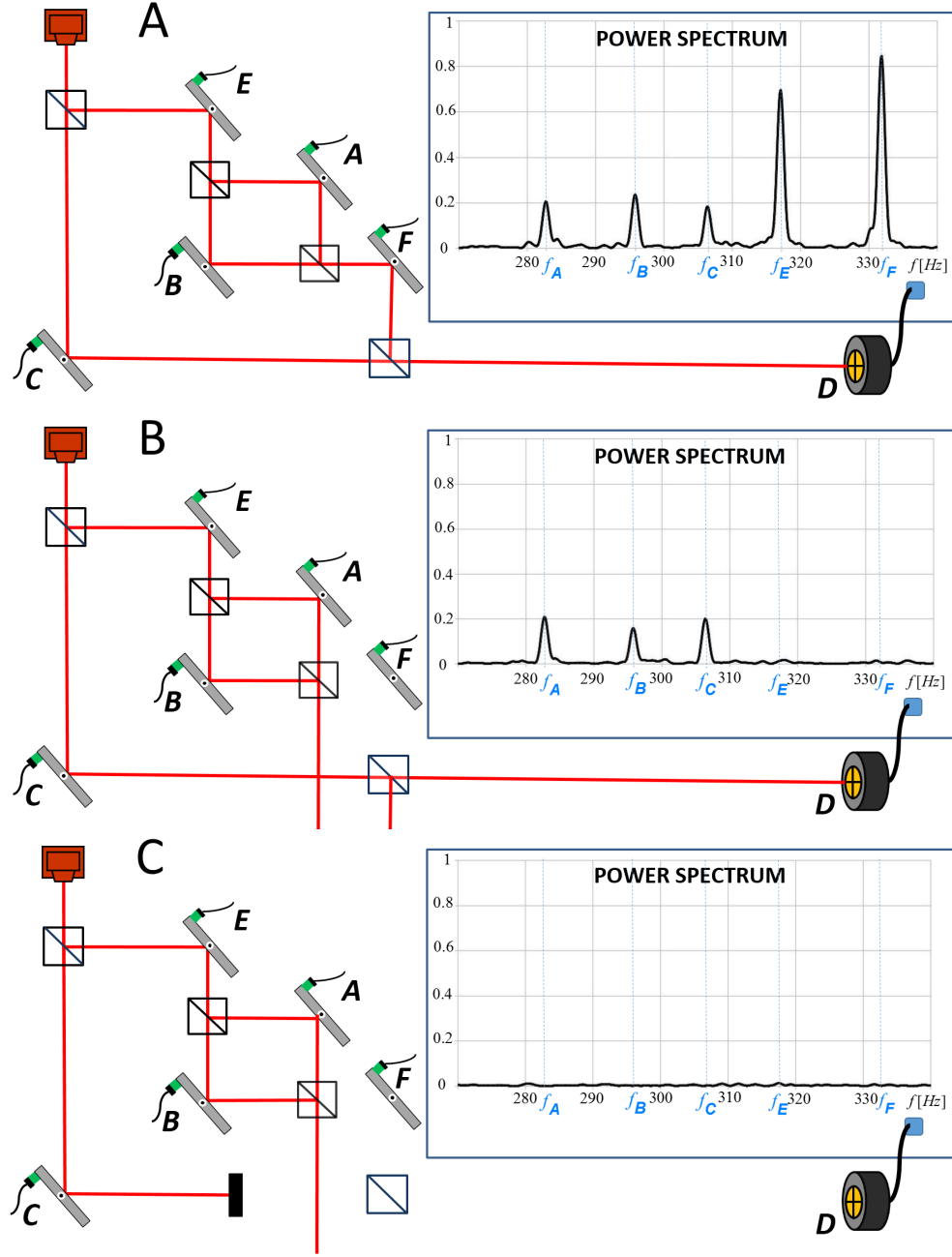


FIG. 2: (A) Measured power spectrum of the signal from the quad-cell photo detector shows frequencies of oscillation of all internal mirrors of the interferometer. (B) When the inner interferometer is tuned in such a way that the beam of light passing through it does not reach the photo-detector, the power spectrum of the signal in the photo-detector still shows frequencies of the mirrors of this interferometer. (C) These frequencies (and all other signals) disappear when we, without changing anything in the upper arm, block the lower arm of the large interferometer.

evolving wave near F explains why we do not see a peak at f_F . This picture also explains the power spectrum in Fig. 1A,B, Fig. 2A. and tells us that blocking mirror F should eliminate peaks at frequencies f_A and f_B [14].

Let us describe the experiment depicted in Fig. 2B in the framework of the TSVF in more detail. The two-state vector of the photon at the moment that its partial wave packets bounce off the mirrors A , B and C is

$$\langle \Phi | \Psi \rangle = \frac{1}{\sqrt{3}} (\langle A | + i \langle B | + \langle C |) \quad \frac{1}{\sqrt{3}} (|A \rangle + i |B \rangle + |C \rangle), \quad (1)$$

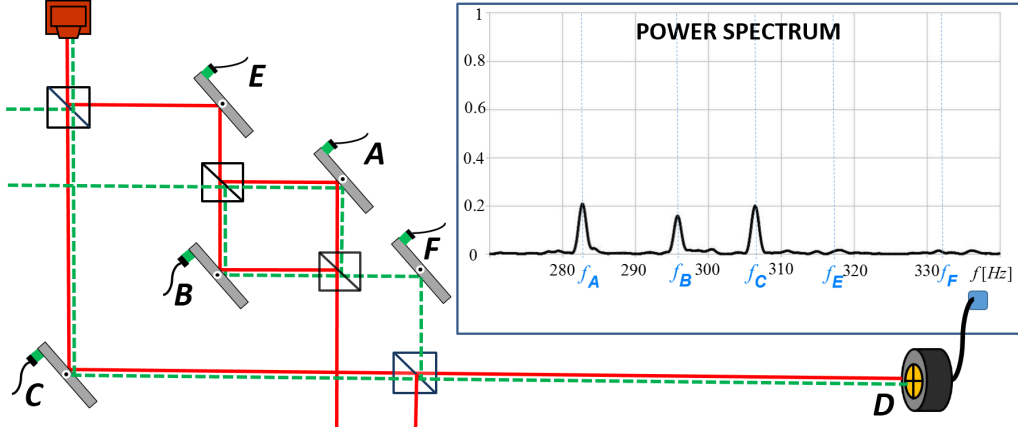


FIG. 3: The two-state vector description of the photon inside the interferometer includes the standard forward evolving quantum state (red line) and backward evolving quantum state (green dashed line) of the photon detected by the quad-cell photo-detector. It provides an explanation of the observed power spectrum: frequencies f_C , f_A and f_B are present while f_E and f_F are not. The photon was present only where both forward and backward quantum wave functions do not vanish.

where we used natural notation: $|A\rangle$ is a localized wave packet near mirror A , etc. (Note that an equivalent two-state vector describes the particle in the so called “Three-box paradox” [15].)

The main result of the TSVF is that any weak enough coupling to a variable O of a pre- and postselected system results in an effective coupling to the *weak value* of O :

$$O_w \equiv \frac{\langle \Phi | O | \Psi \rangle}{\langle \Phi | \Psi \rangle}. \quad (2)$$

The rotation of a mirror makes the photon itself the measuring device of its projection operator on the location of the mirror. Since the amplitude of the vibration of the mirrors is $\sim 1.5 \cdot 10^{-7} \text{ rad}$ while the quantum uncertainty of the direction of the photon is $\sim 3.7 \cdot 10^{-4} \text{ rad}$, this is a *weak measurement* of the projection. The pointer variable is the transverse momentum of the photon which is transformed to a spatial shift at the detector. Using (8) and (2) we calculate the weak values of the projection operators at all mirrors A , B and C :

$$(\mathbf{P}_A)_w = (\mathbf{P}_C)_w = 1, \quad (\mathbf{P}_B)_w = -1, \quad (\mathbf{P}_E)_w = (\mathbf{P}_F)_w = 0. \quad (3)$$

This explains the equal peaks at frequencies f_A , f_B , and f_C and the absence of peaks at f_E and at f_F in Fig. 3. The peak at f_B is the same as at f_A and f_C because the power spectrum shows only the size of the signal, not its sign. Weak value analysis of the results in other setups presented in Supplement II [16].

Let us describe now the experimental details. The nested MZI inside the upper arm of the large interferometer is constructed from two non-polarizing beam splitters and two mirrors, Fig. 4. The interference in this MZI is controlled by translating mirror B and monitoring the output signal at the left port of BS_2 using a photo-detector (PD). The measured interference visibility of the inner MZI is about 98.5%. For the external interferometer, 1:2 beam splitters are implemented utilizing polarizers and polarization beam splitters. The input beam is produced using a continuous wave diode laser (LD) ($\sim 785 \text{ nm}$ Thorlabs-L785P090) and a Faraday isolator (FI) which cancels back reflections. Using an attenuator, the intensity of the input beam was reduced by a factor of 3 for the setup with constructive interference, Fig. 2A, relative to the scheme with destructive interference, Fig. 2B. The beam is spatially filtered and shaped to a $\sim 1 \text{ mm}$ waist Gaussian beam using a single-mode fiber followed by a beam contraction telescope. A quarter-wave plate, a half-wave plate, and a Glan-Taylor polarizer P_1 cancel the birefringence introduced by the fiber, and produce a beam with a linear polarization at angle 54.7° , which leads to an intensity ratio of 2 at the output ports of polarization beam splitter PBS_1 . The beam recombines at a polarization beam splitter PBS_2 , and is postselected using polarizer P_2 , also at angle 54.7° . Mirrors A , B , C , E and F are mounted on piezo-electrically-driven mirror mounts (PZMs), and weak sinusoidal modulations of the tilts around the horizontal axes are used to introduce vertical shifts of the beam reaching the quad-cell photo-detector (QCD) (First Sensor QP50-6-SD2). Each mirror is seeded with a different sine frequency voltage ($\sim 200 \text{ mVpp}$) that results in small amplitude oscillations ($\sim 300 \text{ nrad}$) of the reflected beam. At the output of the interferometer we measured the vertical position of the beam using QCD placed at a distance of $\sim 2 \text{ m}$ from the interferometer. The size of the beam on the detector is $\sim 1.2 \text{ mm}$

and the displacement caused by the mirrors oscillations is about $\sim 600nm$. The QCD signal was sampled using a data acquisition card (NI USB-6008) at a rate of $2.5KHz$ during 1 second intervals. We perform harmonic analysis using MATLAB, and create smoothed power spectra of the signals, Figs. 1, 2.

Before each data acquisition run, the phase of the nested interferometer was precisely adjusted using a computer-controlled algorithm which brought the intensity at the auxiliary detector PD to minimum (or maximum) by varying the position of mirror B using its PZM. During the one second of each data acquisition run the mirror position was kept fixed, but the phase remained stable. The stability was ensured by preliminary stability analysis [17] and observation of the constant intensity at PD during the run. The phase in the external interferometer was manually tuned before each run - it was not crucial to precisely adjust this phase since it only affected the magnitude of the peaks in the spectrum but not their presence.

Note that the QCD senses photons coming from a wide angle, so the backward evolving state of the detected photon is much wider than what is shown on Fig. 3, but this does not change the argument: the backward evolving quantum wave is not reflected off the mirror E .

Our interference experiments utilize visible light with about 10^{14} photons at each run. Thus, even Maxwell's equations for the classical electromagnetic field should explain the observed phenomena. Indeed, the TSVF adds no new predictions beyond standard quantum mechanics. It just provides a simple intuitive picture of pre- and postselected quantum systems. In the standard framework of quantum mechanics it is not easy to foresee these effects, but when the question is asked, the calculation is straightforward. The effect is due to a tiny leakage of light in the inner interferometer. Essentially, the same explanation holds also for a classical electromagnetic wave. The field entering the interferometer is well characterized by a Gaussian $\Psi(x, y) = \mathcal{A}e^{-\frac{x^2+y^2}{2\Delta^2}}$. The beam can reach the quad-cell detector D passing through the three arms A , B and C . In the setup described in Fig. 2A the fields passing through the different arms all reach the plane of the quad-cell detector with the same phase, while in Fig. 2B the field passing through arm B gets a relative phase π . Due to the beam splitters on the way, the amplitudes of the beams passing through each arm are reduced by a factor of 3. Due to the vibration of their angles, the mirrors cause shifts of the beams in the y direction such that beam C is shifted by δ_C , beam A by $\delta_E + \delta_A + \delta_F$, and beam B by

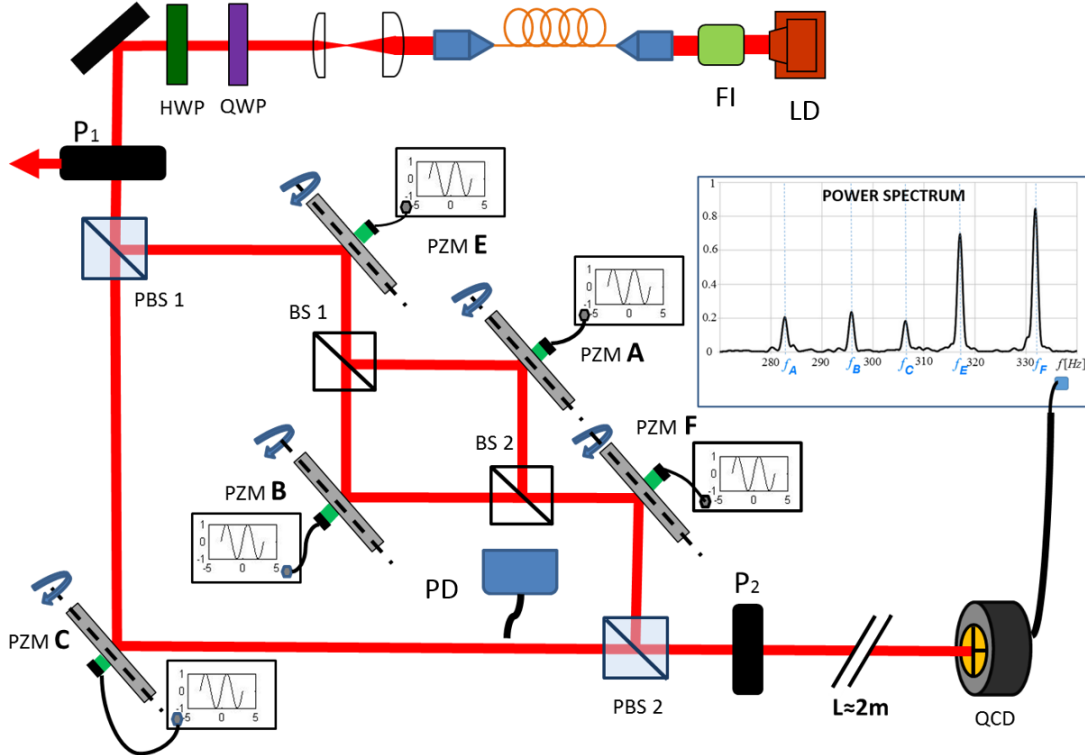


FIG. 4: Detailed experimental setup.

$\delta_E + \delta_B + \delta_F$. Thus, in the setup of Fig. 2B, the field on the detector, $\Psi(x, y)$, is:

$$\frac{\mathcal{A}}{3} \left(e^{-\frac{x^2 + (y - \delta_C)^2}{2\Delta^2}} + e^{-\frac{x^2 + (y - \delta_E - \delta_A - \delta_F)^2}{2\Delta^2}} - e^{-\frac{x^2 + (y - \delta_E - \delta_B - \delta_F)^2}{2\Delta^2}} \right). \quad (4)$$

The difference of the integrals of the intensity over the regions $y > 0$ and $y < 0$ is our signal:

$$\int_{y>0} |\Psi(x, y)|^2 dx dy - \int_{y<0} |\Psi(x, y)|^2 dx dy. \quad (5)$$

Since all the shifts are small, $\delta \ll \Delta$, only the first order in δ is considered. Substituting (4) in (21) we obtain that the signal is proportional to $\delta_C + \delta_A - \delta_B$, in agreement with (15). Every δ has its own frequency and this explains the observed power spectrum of the signal [18].

It will be of interest to repeat this experiment in a regime where neither a classical wave evolution description nor a single particle quantum wave description can provide an explanation. One challenging proposal is to perform the same interference experiment with neutrons. A conceptually different approach aiming to find out where were the particles inside an interferometer would be a weak measurement using an external measuring device. Kerr media provides an interaction between photons, and a weak measurement of a projection operator of a single photon is considered feasible [19] for amplified weak values, which, however, is not the case in our setup.

In conclusion, we have performed direct measurements which shed new light on the question: Where were the photons passing through an interferometer? The main results are presented in Fig. 2B. The photons themselves tell us where they have been. And the story they tell is surprising. The photons do not always follow continuous trajectories. Some of them have been inside the nested interferometer (otherwise they could not have known the frequencies f_A, f_B), but they never entered and never left the nested interferometer, since otherwise they could not avoid the imprints of frequencies f_E and f_F of mirrors E and F leading photons into and out of the interferometer. Only the description with both forward and backward evolving quantum states provides a simple and intuitive picture of pre- and postselected quantum particles.

Acknowledgements. This work has been supported in part by the Binational Science Foundation Grant No. 32/08, the Israel Science Foundation Grant No. 1125/10 and Sackler Institute of Condense Matter Equipment Grant.

-
- [1] L. Vaidman, Phys. Rev. A, **87**, 052104 (2013).
 - [2] T. J. Herzog, P. G. Kwiat, H. Weinfurter, and A. Zeilinger, Phys. Rev. Lett. **75**, 3034 (1995).
 - [3] V. Jacques, *et al.*, Science **315**, 966 (2007).
 - [4] A. Peruzzo, *et al.*, Science **338**, 634 (2012).
 - [5] F. Kaiser, *et al.*, Science **338**, 637 (2012).
 - [6] K.J. Resch, J.S. Lundeen, A.M. Steinberg, Phys. Lett. A, **324**, 125 (2004).
 - [7] S. Kocsis *et al.*, Science **223** 1170 (2011).
 - [8] A. Matzkin, Phys. Rev. Lett. **109**, 150407 (2012).
 - [9] O. Hosten *et al.*, Nature **439**, 949 (2006).
 - [10] L. Vaidman, Phys. Rev. Lett. **98**, 160403 (2007).
 - [11] Y. Aharonov, P. G. Bergmann and J. L. Lebowitz, Phys. Rev. B **134**, 1410 (1964).
 - [12] Y. Aharonov and L. Vaidman, Phys. Rev. A **41**, 11 (1990).
 - [13] P. Grangier, G. Roger and A. Aspect, Europhys. Lett. **1**, 173 (1986).
 - [14] Supplement I: The TSVF analysis of setups Fig 1. A,B and Fig. 2 A,C and additional measurement with mirror F blocked.
 - [15] Y. Aharonov and L. Vaidman, J. Phys. A **24**, 2315 (1991).
 - [16] Supplement II: Weak value analysis of setups Fig 1. A,B and Fig. 2 A,C.
 - [17] Supplement III: Stability analysis of the inner interferometer.
 - [18] Supplement IV: Computer calculations of the expected experimental results.
 - [19] A. Feizpour, X. Xing, and A. M. Steinberg, Phys. Rev. Lett. **107**, 133603 (2011).

Supplement I

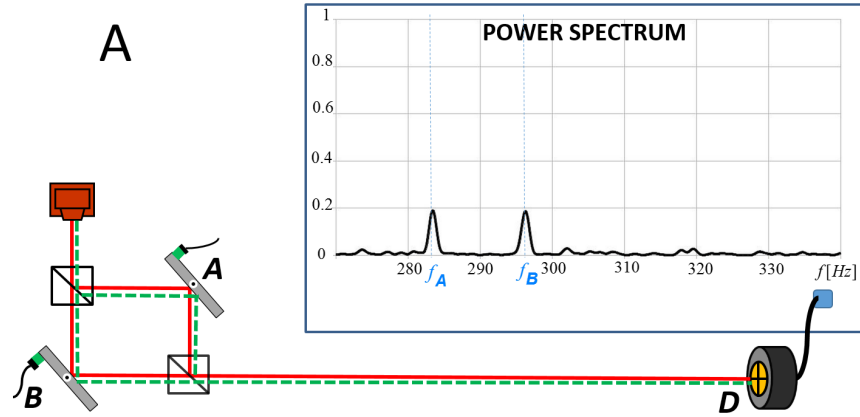


FIG. 5: Setup of Fig. 1A. The two-state vector description of the photon inside the interferometer includes the standard forward evolving quantum state (red line) and backward evolving quantum state (green dashed line) of the photon detected by the quad-cell photo-detector. It provides an explanation of the observed power spectrum: frequencies f_A and f_B appear.

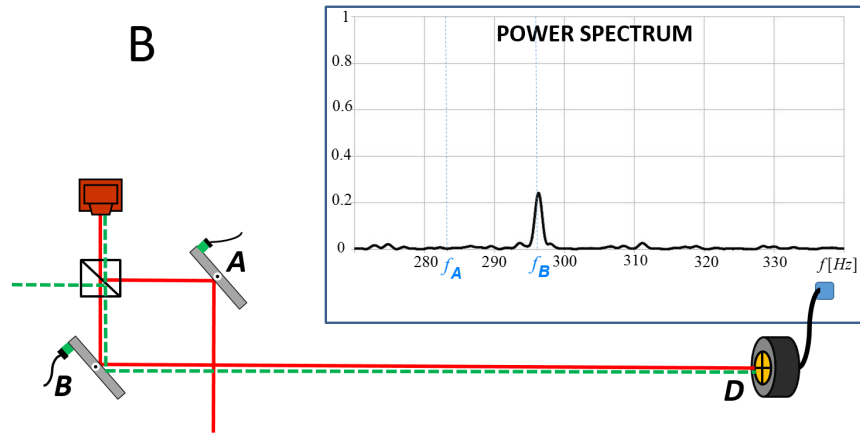


FIG. 6: Setup of Fig. 1B. The forward evolving and the backward evolving quantum states are present together only at mirror B: only the peak at frequency f_B appears.

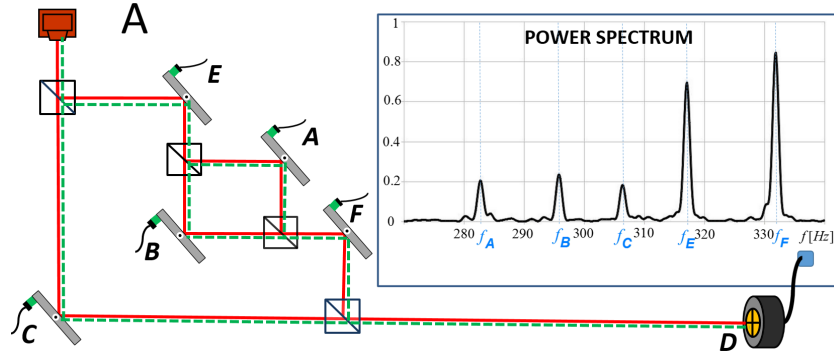


FIG. 7: Setup of Fig. 2A. The forward and backward evolving states are present together in all mirrors: peaks at all frequencies appear.

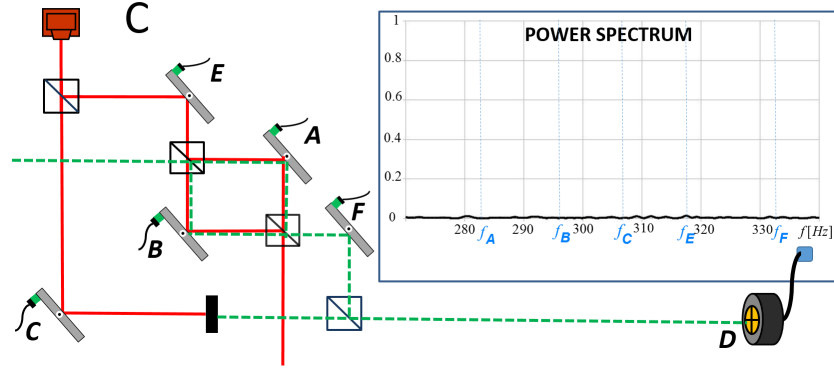


FIG. 8: Setup of Fig. 2C. The forward evolving and the backward evolving quantum states are present together at mirrors *A* and *B*, but no peaks are present! The (leaking) photons which do reach the detector are shifted with corresponding frequencies, we just do not get enough photons at the detector to see anything above the noise.

Additional measurement with mirror *F* blocked

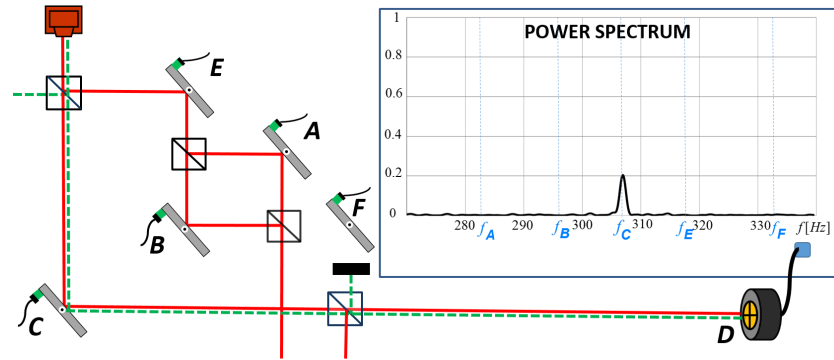


FIG. 9: The forward and backward evolving states are present together only at mirror *C* and thus, the only peak in the power spectrum is at f_C . Since according to the naive approach the presence of peaks at f_A and f_B in Fig. 2B is very counterintuitive, one might suspect that these peaks may result from some unrelated electronic noise. A block between mirror *F* and the last beam splitter absorbs the backward evolving wave moving towards mirrors *F*, *A*, *B*, and *E*. In the language of forward wave function only, it absorbs the leakage of the wave from the inner interferometer. Thus theoretically, according to the standard and the TSVF approaches, the block ensures the absence of peaks at the corresponding frequencies. Therefore, this experiment provides a decisive test for the absence of electronic noise in Fig. 2B.

Supplement II

Weak value analysis of setups Fig. 1A,B and Fig. 2A,C

The main result of the Letter is the presence of the photon near mirrors A and B in the setup of Fig. 2B. as discussed in the Letter itself. However, it is also of interest to understand the presence and the size of the observed peaks in other setups.

The two state vector of the photon in the setup of Fig. 1A at the intermediate time is:

$$\langle \Phi | \Psi \rangle = \frac{1}{\sqrt{2}} (\langle A | + \langle B |) \frac{1}{\sqrt{2}} (|A\rangle + |B\rangle), \quad (6)$$

Thus, the weak values of the projections on the locations of the photon at the mirrors are

$$(\mathbf{P}_A)_w = (\mathbf{P}_B)_w = \frac{1}{2}. \quad (7)$$

This explains the equal size peaks at f_A and f_B .

The two state vector of the photon in the setup of Fig. 1B at the intermediate time is:

$$\langle \Phi | \Psi \rangle = \frac{1}{\sqrt{2}} (\langle A | + \langle B |) |B\rangle, \quad (8)$$

Thus, the weak value of the projections on the location at the mirrors are

$$(\mathbf{P}_A)_w = 0, \quad (\mathbf{P}_B)_w = 1. \quad (9)$$

This explains why there is only one peak at f_B . Due to oscillations of mirror B , the shift of the beam is twice as large as in the setup of Fig. 1A. However, the measured signal is the same since it is also proportional to the total intensity on the quad-cell detector which is half relative to the case of Fig. 1A.

The two state vector of the photon in the setup of Fig. 2A at the intermediate time is:

$$\langle \Phi | \Psi \rangle = \frac{1}{\sqrt{3}} (\langle A | + \langle B | + \langle C |) \frac{1}{\sqrt{3}} (|A\rangle + |B\rangle + |C\rangle), \quad (10)$$

Thus, the weak value of the projections on the location of the photon at mirrors A , B , and C are:

$$(\mathbf{P}_A)_w = (\mathbf{P}_C)_w = (\mathbf{P}_B)_w = \frac{1}{3}. \quad (11)$$

At an earlier time, when one of the wave packets is near mirror E , the two state vector is:

$$\langle \Phi | \Psi \rangle = \frac{1}{\sqrt{3}} (\sqrt{2}\langle E | + \langle C |) \frac{1}{\sqrt{3}} (\sqrt{2}|E\rangle + |C\rangle), \quad (12)$$

Thus, the weak value of the projection on the location at the mirror E is:

$$(\mathbf{P}_E)_w = \frac{2}{3}. \quad (13)$$

In a similar way we obtain

$$(\mathbf{P}_F)_w = \frac{2}{3}. \quad (14)$$

These results explain why there are peaks at all frequencies. The peaks at f_E and f_F are four times larger than the peaks at f_A , f_B and f_C because in the definition of the power spectrum, the power is proportional to the square of the signal. The size of the peaks at f_A , f_B and f_C are the same (up to noise) as in the setup of Fig. 2B in spite of the fact that the weak value (and thus the shift of the beam) is smaller by the factor of 3. This is because the intensity in the setup of Fig. 2A is 3 times larger. (It had to be 9 times larger but the input intensity was reduced by the factor of 3).

The two-state vector of the photon in the setup of Fig. 2C (Fig. 4 of Supplement 1) at the intermediate time is:

$$\langle \Phi | \Psi \rangle = \frac{1}{\sqrt{3}} (\langle A | + i \langle B | + \langle Absorbed |) \frac{1}{\sqrt{3}} (|A\rangle + i|B\rangle + |C\rangle), \quad (15)$$

In this situation the weak values are not defined: the post-selected state is orthogonal to the forward evolving state. This means that in the ideal case there are no such pre- and post-selected photons. This explains why we have seen the null result. (The formalism can deal with a realistic case in which the leakage from the inner interferometer will make the weak values well defined.)

Supplement III

Stability analysis of the inner interferometer

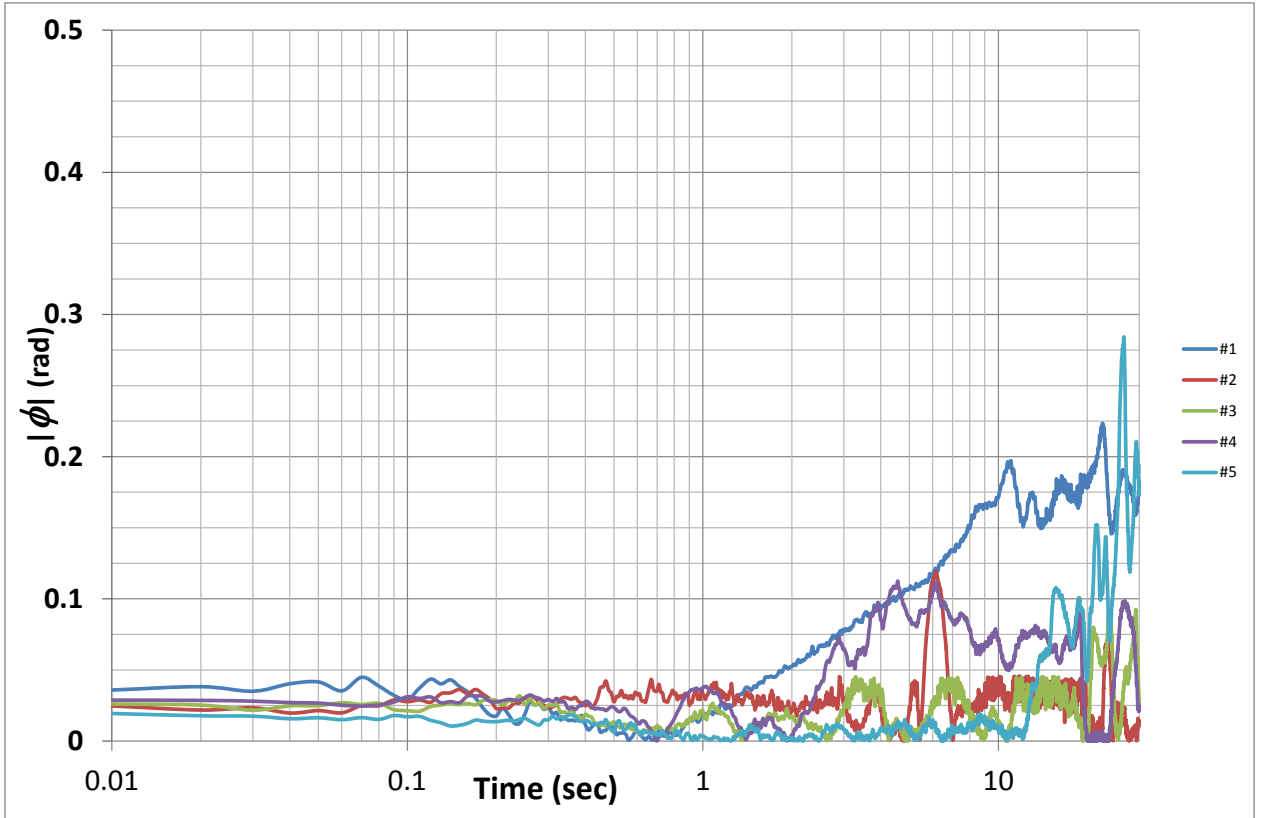


FIG. 10: The absolute value of the phase (calculated based on the intensity measured in the auxiliary detector PD) in five 30-seconds runs. Each run started automatically when the computer-controlled algorithm brought the intensity close to minimum. The results show a reliable action of the algorithm that adjust the phase to zero, and the high stability during the first second of passive stabilization - the duration of each run.

Supplement IV

Computer calculations of the expected experimental results

Here we present direct calculations of the expected experimental results based on the standard quantum formalism which is the same as in classical electromagnetic waves theory.

We model the field entering the interferometer as a Gaussian

$$\Psi(x, y) = \mathcal{A}e^{-\frac{x^2 + y^2}{2\Delta^2}}. \quad (16)$$

We model displacement of the beam on the plane of the quad-cell detector due to rotation of a mirror X as

$$\delta_X = \delta \sin(2\pi f_X t). \quad (17)$$

The parameters corresponding to our experiment are:

$$\Delta = 1.2mm, \quad \delta = 0.6\mu m, \quad (18)$$

$$f_A = 282Hz, \quad f_B = 296Hz, \quad f_C = 307Hz, \quad f_E = 318Hz, \quad f_F = 332Hz. \quad (19)$$

We start with the setup described in Fig. 2B. The field on the detector is given by Eq. (4) in the Letter:

$$\Psi(x, y) = \frac{\mathcal{A}}{3} \left(e^{-\frac{x^2 + (y - \delta_C)^2}{2\Delta^2}} + e^{-\frac{x^2 + (y - \delta_E - \delta_A - \delta_F)^2}{2\Delta^2}} - e^{-\frac{x^2 + (y - \delta_E - \delta_B - \delta_F)^2}{2\Delta^2}} \right). \quad (20)$$

Our signal is the difference of the integrals of the intensity over the regions $y > 0$ and $y < 0$:

$$S \equiv \int_{y>0} |\Psi(x, y)|^2 dx dy - \int_{y<0} |\Psi(x, y)|^2 dx dy. \quad (21)$$

We have calculated the signal at a rate of $2.5KHz$ during 1 second interval. We performed a harmonic analysis using MATLAB and created smoothed power spectrum of the signal averaging on every 10 points, exactly as in the analysis of the real data.

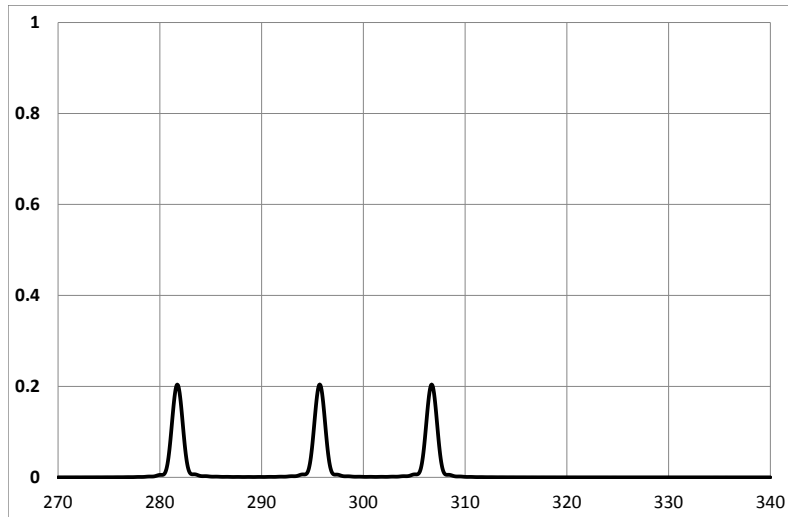


FIG. 11: Calculated Power Spectrum of the signal in the setup described in Fig. 2B.

We repeated this calculation for the setup of Fig. 2C. The field on the detector in this case is:

$$\Psi(x, y) = \frac{\mathcal{A}}{3} (e^{-\frac{x^2 + (y - \delta_E - \delta_A - \delta_F)^2}{2\Delta^2}} - e^{-\frac{x^2 + (y - \delta_E - \delta_B - \delta_F)^2}{2\Delta^2}}). \quad (22)$$

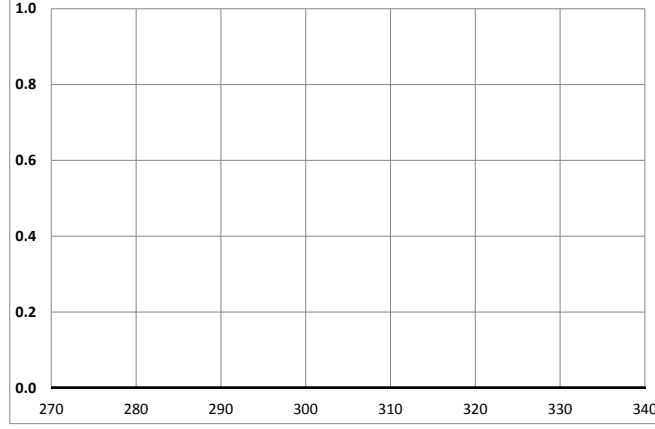


FIG. 12: Calculated Power Spectrum of the signal in the setup described in Fig. 2C.

We repeated this calculation for the setup of Fig. 2A. corresponding to constructive interference. In order to reduce the difference of intensities at the detector between the runs with constructive and destructive interference (a factor of 9) we attenuated the intensity here by a factor of 3. The field in this case is:

$$\Psi(x, y) = \frac{\mathcal{A}}{3\sqrt{3}} (e^{-\frac{x^2 + (y - \delta_C)^2}{2\Delta^2}} + e^{-\frac{x^2 + (y - \delta_E - \delta_A - \delta_F)^2}{2\Delta^2}} + e^{-\frac{x^2 + (y - \delta_E - \delta_B - \delta_F)^2}{2\Delta^2}}). \quad (23)$$

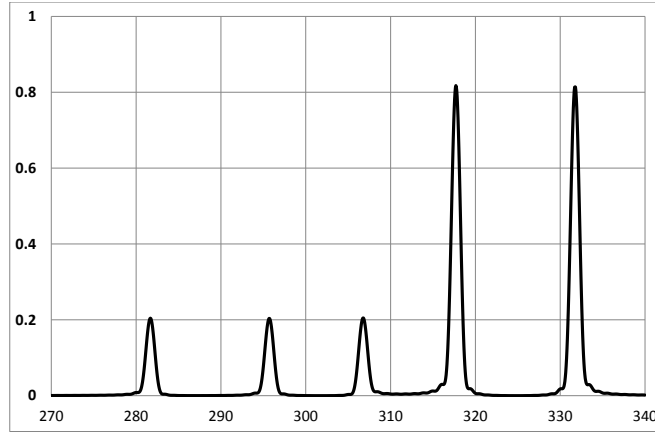


FIG. 13: Calculated Power Spectrum of the signal in the setup described in Fig. 2A.